Are we seeing accretion flows in a 250 kpc Lyα halo at z = 3?

J. Vernet, M. D. Lehnert, C. de Breuck, M. Villar-Martín, D. Wylezalek, T. Falkendal, G. Drouart, S. Kolwa, A. Humphrey, B. P. Venemans, et al.

Astronomy
&
Astrophysics

LETTER TO THE EDITOR

Are we seeing accretion flows in a 250 kpc Lyα halo at *z = 3*?[★]

J. Vernet[1], M. D. Lehnert[2], C. De Breuck[1], M. Villar-Martín[3], D. Wylezalek[4], T. Falkendal[1,2], G. Drouart[5], S. Kolwa[1], A. Humphrey[6], B. P. Venemans[7], and F. Boulanger[8,★★]

[1] European Southern Observatory, Karl-Schwarzschild-Str. 2, 85748 Garching, Germany
e-mail: jvernet@eso.org
[2] Sorbonne Universités, UPMC, Paris VI, CNRS UMR 7095, Institut d'Astrophysique de Paris, 98bis Bd Arago, 75014 Paris, France
[3] Centro de Astrobiologìa (INTA-CSIC), Carretera de Ajalvir, km 4, 28850 Torrejòn de Ardoz, Madrid, Spain
[4] Department of Physics and Astronomy, Johns Hopkins University, 3400 N. Charles St, Baltimore, MD 21218, USA
[5] International Centre for Radio Astronomy Research, Curtin University, Perth WA 6845, Australia
[6] Instituto de Astrofísica e Ciências do Espaço, Universidade do Porto, CAUP, Rua das Estrelas, 4150-762 Porto, Portugal
[7] Max-Planck Institute for Astronomy, Königstuhl 17, 69117 Heidelberg, Germany
[8] Institut d'Astrophysique Spatiale, 91405 Orsay, Université Paris Sud et CNRS, France

ABSTRACT

Using MUSE on the ESO-VLT, we obtained a four-hour exposure of the $z = 3.12$ radio galaxy MRC 0316-257. We detect features down to $\sim 10^{-19}$ erg s^{-1} cm^{-2} arcsec^{-2}, with the highest surface brightness regions reaching more than a factor of 100 higher. We find Lyα emission out to $\sim$250 kpc in projection from the active galactic nucleus (AGN). The emission shows arc-like morphologies arising at 150−250 kpc from the nucleus in projection, with the connected filamentary structures reaching down into the circumnuclear region. The most distant arc is offset by $\sim$700 km s^{-1} relative to circumnuclear HeIIλ1640 emission, which we assume to be at the systemic velocity. As we probe emission closer to the nucleus, the filamentary emission narrows in projection on the sky, the relative velocity decreases to $\sim$250 km s^{-1}, and the line full-width at half maximum ranges from $\sim$300−700 km s^{-1}. From UV line ratios, the emission on scales of 10s of kpc from the nucleus along a wide angle in the direction of the radio jets is clearly excited by the radio jets and ionizing radiation of the AGN. Assuming ionization equilibrium, the more extended emission outside of the axis of the jet direction would require 100% or more illumination to explain the observed surface brightness. High-speed ($\gtrsim$300 km s^{-1}) shocks into rare gas would provide sufficiently high surface brightness. We discuss the possibility that the arcs of Lyα emission represent accretion shocks and the filamentary emission represents gas flows into the halo, and compare our results with gas accretion simulations.

Key words. galaxies: evolution – galaxies: high-redshift – galaxies: active – galaxies: ISM – galaxies: halos

1. Introduction

High-redshift radio galaxies, quasars (Heckman et al. 1991a,b), QSOs (Christensen et al. 2006), and "Lyα blobs" (Steidel et al. 2000) exhibit strong, extended Lyα emission. High-redshift radio galaxies play a central role in our evolving understanding of the association between massive galaxies, their clustered environments, and halo gas. The first galaxies at high redshift, $z > 2$, where halo gas was detected in Lyα emission over scales of 10−100s kpc, were radio galaxies (Chambers et al. 1990). These Lyα halos are generally aligned with the radio jets but extend well beyond the radio lobes (Villar-Martín et al. 2003). The association between the active galactic nuclei (AGN) and the extended Lyα emission is unclear. In the circumgalactic environment within the radius subtended by the radio lobes, the Lyα kinematics are complex, while outside the radio emission, the gas is relatively quiescent (Villar-Martín et al. 2003).

The energy sources of Lyα nebulae are poorly constrained (Cantalupo 2017). All processes that excite the Lyα emission depend on the distribution of the emission line gas, the type of objects within the nebula, and on how far away the emission is located from sources of ionizing photons. While ionizing photons from galaxies embedded within the Lyα emission are a plausible explanation (Overzier et al. 2013), other sources powering the Lyα emission include ionization by the meta-galactic flux, mechanical heating, dissipation of potential energy as the gas falls into the halo, and resonance scattering of Lyα and UV continuum photons. The mechanisms powering the emission are inextricably linked with the origin of the gas. If the emission is related to outflows, the excitation of the gas might be due to shocks and ionization by stars or AGN (Swinbank et al. 2015). If the gas extends >100 kpc, it may be accreting from the cosmic web or gas instabilities in the halo (Maller & Bullock 2004). In this case, we expect the emission to be due to mechanical heating associated with accretion shocks (Birnboim & Dekel 2003) or from the dissipation of potential energy that the flows gain as they fall into the potential.

While these general arguments motivated us to obtain deep integral-field spectroscopy of radio galaxies using MUSE on the ESO-VLT, in the specific case of MRC 0316-257, we are motivated by its striking Lyα morphology. MRC 0316-257 is a well-studied massive $\approx 2 \times 10^{11}$ $M_\odot$ radio galaxy (De Breuck et al. 2010) that lies in a galaxy overdensity

Table 1. Characteristics of spectra of particular regions.

Id	SB × 10^{-19} erg s^{-1} cm^{-2} arcsec^{-2}	ΔV km s^{-1}	*FWHM* km s^{-1}	Area arcsec^2
1	1.3 ± 0.2	142 ± 13	250 ± 32	14.3
2	1.6 ± 0.1	220 ± 9	430 ± 21	46.5
3	1.4 ± 0.1	211 ± 12	550 ± 29	40.5
4	5.5 ± 0.2	224 ± 5	410 ± 13	9.3
5	2.8 ± 0.1	225 ± 11	550 ± 26	11.4
6	2.1 ± 0.1	230 ± 6	395 ± 16	43.4
7	0.8 ± 0.1	227 ± 25	525 ± 62	35.0
8	0.9 ± 0.1	226 ± 28	670 ± 70	17.2
9	2.6 ± 0.2	250 ± 14	510 ± 32	8.5
10	0.8 ± 0.1	290 ± 13	510 ± 32	74.0
11	1.9 ± 0.1	610 ± 11	720 ± 27	36.6

Notes. The identification numbers correspond to the regions in Fig. 2. The measured ΔV of regions 2−9 are statistically the same.
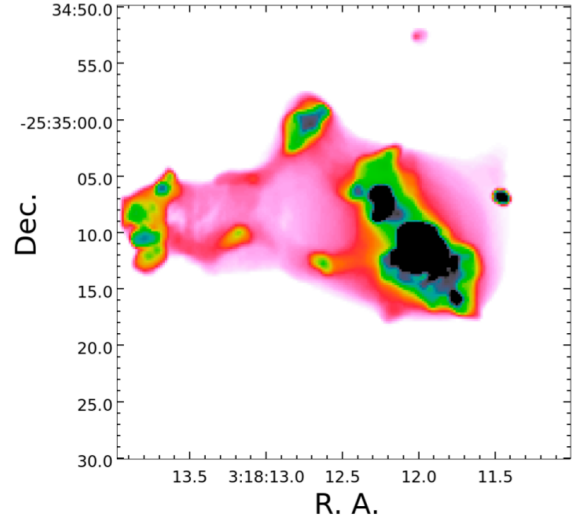

Fig. 1. Narrow-band image 25 Å wide centered on Lyα extracted from an adaptively smoothed datacube with the algorithm described in Martin et al. (2014). We used a maximum spatial smoothing scale of 14″ and a signal-to-noise ratio threshold of 2.5 in making this image. This plot is intended to be illustrative and was not used in the analysis.

(Kuiper et al. 2012). The Lyα emission around MRC 0316-257 is filamentary on scales of ~250 kpc and has a morphology and surface brightness distribution similar to those seen in galaxy simulations. Simulations of gas accretion imply that streams will be visible via their Lyα emission if we detect down to a surface brightness of ≈10^{-19} erg s^{-1} cm^{-2} arcsec^{-2} at $z \sim 3$ (Rosdahl & Blaizot 2012). It is not clear whether these simulations capture all the physics necessary to model the emission and evolution of the accreting gas (e.g., Cornuault et al. 2016). Observational constraints are needed. Of course, one must worry about expectation bias (Jeng 2006). Do we call what we observe a "stream" because its morphology agrees with the results of simulations? While we are concerned about this bias, it is still instructive to compare our results with those of simulations.

2. Observations, analysis, and results

Multi Unit Spectroscopic Explorer (MUSE; Bacon et al. 2010) observations of MRC 0316-257 were obtained in service mode between UT January 2015 14 and 17. We used the Wide Field Mode (1′ × 1′ field of view) with the second-order blocking filter, resulting in a wavelength coverage of 480−935 nm. Our eight 900 s exposures were taken at position angles of 0, 90, 180, and 270° with a small pointing offset to mitigate systematic artifacts. We processed the data using MUSE pipeline version 1 (Weilbacher et al. 2012) to produce a fully calibrated (wavelength, flux, and astrometry) sky-subtracted data cube. The measured image quality of the reconstructed white-light image is ~1″. To preserve any possible extended low surface-brightness features, we did not use sky-residual cleaning algorithms.

To remove remaining artifacts, we subtracted all continuum sources from the datacube using a linear interpolation between two bins 50 Å wide on both sides of the emission line. The very extended Lyα emission is only marginally detected. To make the Lyα morphology more evident, we implemented our own version of the algorithm of Martin et al. (2014, Fig. 1). To provide the characteristics of the Lyα emission, we extracted and fit the Lyα line from several regions (Table 1, Fig. 2). The line ratios of Lyα, CIV$\lambda\lambda$1548, 1551, HeIIλ1640, and CIII]$\lambda\lambda$1907, 1909 of the highest surface brightness regions (3−5) imply they are ionized by the AGN. Beyond the circumnuclear emission, ≳10″ from the AGN, the Lyα emitting regions are too faint to determine line ratios necessary to constrain the ionization source.

We find Lyα emission down to ≈10^{-19} erg s^{-1} cm^{-2} and up to ~35″ from the radio galaxy (~250 kpc in projection). The morphology of the emission, outside of the emission that is likely to be excited by the AGN, is arc- and stream-like, with the higher surface brightness arcs appearing at ~150−250 kpc (regions 1, 2, and 11) from the nucleus, with the connected filamentary structures reaching into the circumnuclear regions (regions 6−8). The most distant arc (region 11) has an offset velocity relative to the arcsecond-scale HeIIλ1640 emission from the AGN of ~700 km s^{-1}. We assumed that the velocity of the HeII line represents the systemic velocity of the system. This assumption is supported by the low relative offset velocity (≲50 km s^{-1}) between circumnuclear dense gas (from CO(8−7)) and HeII in another radio galaxy (Gullberg et al. 2016). Closer to the nucleus, the filaments of Lyα emission narrow on the sky, the redshifted offset velocity decreases to ~250 km s^{-1}, the line full-width at half maximum (FWHM) remains very high, reaching up to 700 km s^{-1} and ~50−100 kpc from the nucleus. Throughout the emission, the lines are broad, ~300−700 km s^{-1}.

Projected onto region 11, we find a $z = 3.1245$ galaxy, which we have dubbed the "Arrow" because of its arrow-like morphology in HST/ACS F814W imaging (Fig. 2).

3. Which mechanisms power the Lyα emission?

Photoionization by the AGN or star formation. While the rest-frame UV emission line ratios indicate that the AGN is likely ionizing the gas within several 10s kpc along the direction of the radio jets (regions 3−6), it is not clear whether the AGN could plausibly provide sufficient ionizing photons to explain the surface brightness of the most extended gas. We can estimate the intensity of the radiation field that is necessary to power the Lyα emission observed at distances larger than ~100 kpc. The surface brightness ranges from ~1−4 × 10^{-19} erg s^{-1} cm^{-2} arcsec^{-2} at such large distances (3−10 × 10^{-17} erg s^{-1} cm^{-2} arcsec^{-2} after correcting for surface brightness dimming). Assuming case B recombination, the recombination rate per unit area that is necessary to sustain this surface brightness is $R_{rec} = 4\pi I_{Ly\alpha}/\gamma_{Ly\alpha}$, where $I_{Ly\alpha}$ is the intensity of the Lyα emission
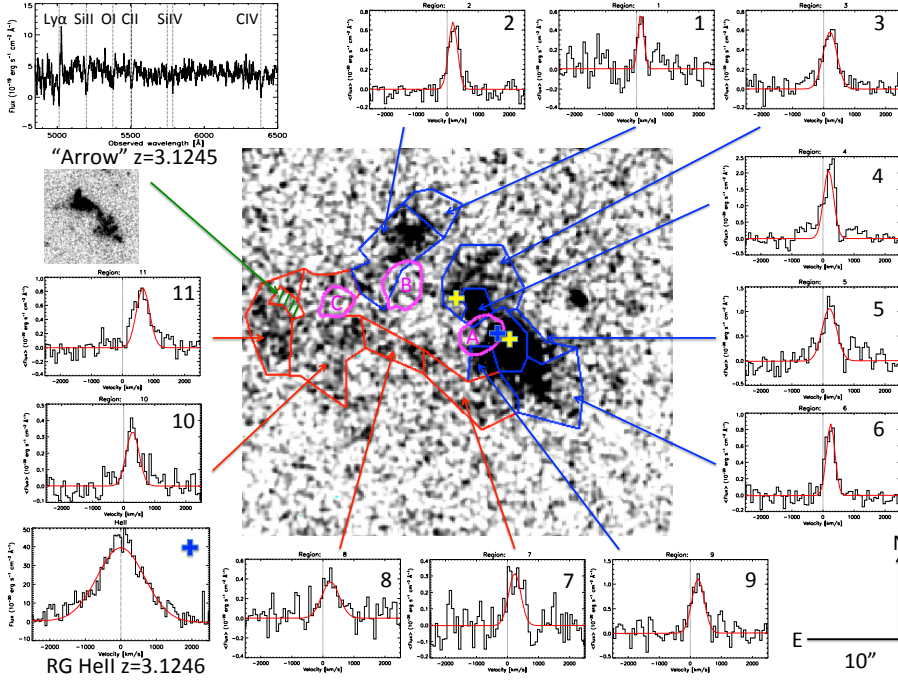
Fig. 2. Grayscale image of the Lyα emission in MRC 0316-257 (scale and orientation at the bottom right). The red and blue lines demarcate 11 regions with their mean Lyα spectra shown in the surrounding plots. The regions bounded by blue lines are probably directly excited by the AGN, while the regions bounded by red lines indicate regions that are perhaps associated with a stream. In each of the spectral plots, we approximate the Lyα profile with the best-fit Gaussian (red). The velocity is relative to systemic (in km s^{-1}; indicated by the black vertical line) measured from the HeII profile (*bottom left*). The purple contours show the region of [OII] emission for three foreground galaxies, labeled A, B, and C, whose redshifts are 0.874, 0.851, and 0.667, respectively. We indicate the positions of the radio lobes (yellow crosses) and AGN (blue cross). The *top two left panels* show the spectrum and HST F814W image of the "Arrow" (green hatched region in the grayscale image).

in photons cm^{-2} s^{-1} sr^{-1} and $\gamma_{Ly\alpha}$ is the number of Lyα photons produced per recombination (0.61). Assuming that every ionizing photon has an energy of 13.6 eV[1] and unity or greater covering fraction, we find that the energy flux necessary to sustain the range of surface brightness we observe is $\approx 0.7-2 \times 10^{-3}$ erg cm^{-2} s^{-1} sr^{-1}.

We used Hβ emission line luminosity as an indicator of the photoionization rate from the AGN and massive stars. The luminosity of Hβ (Nesvadba et al. 2008) implies an ionizing luminosity, $L_{ion} = 4.8 \times 10^{45}$ erg s^{-1}. The ionizing intensity of the AGN at a radius of 100 kpc is $\approx 10^{-3}$ erg s^{-1} cm^{-2} sr^{-1}. The AGN provides sufficient photons to explain the extended Lyα nebula within ~100 kpc, but generally falls short for gas at larger distances. This estimate only applies along lines of sight that are free of intervening absorption and scattering, which may be true within the ionization cone, which is assumed to lie along the radio axes with an opening angle ~45°(blue regions in Fig. 2; Drouart et al. 2012). It is therefore plausible for the gas along the radio jet, even the most extended gas along this direction (regions 1 and 2), to have its surface brightness regulated by the AGN. Away from the ionization cone (red regions 6–11 in Fig. 2), it is unlikely that the AGN provides sufficient photons; young stars embedded in these regions would be an alternative. However, the remarkable uniformity of regions 6–10 suggests that there is no significant local ionization by stars as observed in MRC 0943-242 (Gullberg et al. 2016), for example, and it also argues against a central source such as an AGN ionizing the gas.

Ionization by the meta-galactic flux. At $z \sim 3$, the intensity of ionizing photons due to the meta-galactic flux is $\approx 2 \times 10^5$ photons cm^{-2} s^{-1} (Haardt & Madau 1996). When we assume ionization equilibrium and that the clouds are optically thick, this implies that the meta-galactic ionization rate is about two orders of magnitude lower than the rate necessary to maintain the ionization of the extended gas. This means that while the

meta-galactic flux contributes to the ionization of the diffuse gas, it does not maintain it.

Resonance scattering. If the extended gas has a sufficiently high column of neutral HI to be optically thick at the wavelength of Lyα, then resonance scattering of the Lyα and UV continuum from the AGN can contribute to its surface brightness. The line profiles of the extended Lyα emission do not mirror those of the nuclear gas – they are narrower and have significant velocity offsets relative to the nuclear emission (Table 1). The approximately constant surface brightness of the extended emission argues against a central source exciting the emission. In addition, spectropolarimetry of MRC 0316-257 (Reuland et al. 2003) finds unpolarized (<4%) Lyα emission, arguing against any significant contribution of scattered light to the circumnuclear emission.

Shock heating in the outer halo. Another possibility for exciting the Lyα emission in the halo of MRC 0316-257 is an accretion shock from inflowing gas at the halo boundary and/or shocks from cloud-cloud collisions in a multiphase stream (Cornuault et al. 2016). The morphology of the most extended emission to the west-southwest (region 11) is shell-like and certainly suggestive of compression (a "splash"). We observe a velocity shear between region 11 and that of the inner halo accross regions 6−10 of ~400−500 km s^{-1}. In addition, over regions 6−11, the gas appears to be highly disturbed with FWHM ranging from 300 to 700 km s^{-1}. These violent motions and shears make shock heating a plausible mechanism for exciting the gas.

To test this possibility, we compared our measured surface brightness with those predicted for high-velocity shocks. The models of Allen et al. (2008) imply that even in relatively low-density low-metallicity gas (>few×10^{-3} cm^{-3}), the surface brightness produced by shocks is sufficient to explain our observations for the relative velocities we observe in the data, 300−700 km s^{-1}. Simulations indicate filament densities on the order of 10^{-3} to 10^{-1} cm^{-3} (Rosdahl & Blaizot 2012), in agreement with what is required. The surface brightness is related to the mass flow rate. These densities and velocities imply a mass flow rate, $\rho_{pre-shock} v_{shock} A_{shock} \approx 250 \, M_\odot$ yr^{-1}, for pre-shock density, $\rho_{pre-shock} = 0.01$ cm^{-2}, shock velocity,

---

[1] The photoionization cross-section of hydrogen peaks at 13.6 eV, and this estimate is the maximum number of photons expected. It is therefore an upper limit to the number of photons.

$v_{shock} = 500 \, km \, s^{-1}$, and area, A_{shock}, and for simplicity, of a circle with a radius of 25 kpc.

While we have used the observed high relative velocities and large line widths as a justification to explore the possibility of shock heating, caution is warranted. The relative velocities and large line widths may both be partially due to radiative transfer effects (Cantalupo et al. 2005). The size of the effect depends on whether the medium is multiphasic and on the cause of the ionization. However, none of the Lyα lines in the most extended regions (1, 2, and 6–11) appear split, as might be expected if radiative transfer effects are important.

4. Lyα structures as accretion streams

Comparing the relative velocities of galaxies surrounding MRC 0316-257 with those from cosmological simulations, Kuiper et al. (2012) suggested that it is a result of the ongoing merger of two massive protoclusters of $\sim 10^{14} \, M_\odot$. The combined findings of the surface brightness of the gas in the outer halo, which is is consistent with being shocked heated, its arc- or shell-like and filamentary morphology, large line widths, redshifted velocities, and relatively smooth change in velocity as a function of distance from the AGN suggest that this may be gas accreting from the cosmic web (Rosdahl & Blaizot 2012; Goerdt et al. 2015). If we make this assumption, then what do our results tell us about gas accretion into massive halos, and do they agree with results from cosmological simulations?

For this comparison, we focus exclusively on the filamentary structure to the west-southwest of the AGN (regions 6–11). We limit ourselves to these regions because none of the low surface brightness emission shows obvious evidence for being ionized by the AGN, they do not lie along the direction of the radio jets (which trace the direction of the ionization cone, and the ionization cones have opening angles $\sim 45°$, suggesting these regions lie outside; Drouart et al. 2012), and they extend rather continuously in emission from the outer halo into the circumnuclear region. As we noted in the introduction, these regions have surface brightnesses consistent with estimates from simulations (Rosdahl & Blaizot 2012). The Arrow lies in this structure, which is seen in simulated filaments (Gheller et al. 2016, Fig. 2). These observations form the basis for our assumption that these regions are part of an accretion stream.

The surface brightness of the distant arc can be explained by shock heating. When we assume that such a shock occurs at the virial radius, simple scaling relations imply radii of ~ 150 and 330 kpc for 10^{13} and $10^{14} \, M_\odot$ halos, respectively. Similarly, the virial velocities for halos with these masses are 500 and 1100 $km \, s^{-1}$. We do not necessarily expect the velocities of the streams to be equal to the virial velocity, but they can be as low as half velocity (Goerdt & Ceverino 2015). The distance of the outermost shell from the nucleus and the velocities we observe are both consistent with virial expectations. We observe projected distances and velocities (and the projection of the velocity could change with position), not true positions and velocities, therefore, by necessity, this is only an order-of-magnitude comparison. Simulations do show broad lines in Lyα, on the same order ($100s \, km \, s^{-1}$) as we observe (Goerdt et al. 2010).

Gas accretion through a stream, while able to make up most of the total accretion rate, can also vary substantially within a filament. Goerdt et al. (2015) found accretion rates of $\sim 50 - 5000 \, M_\odot \, yr^{-1} \, sr^{-1}$ through filaments for a halo mass of $\approx 10^{12} \, M_\odot$. Scaling these rates per sr upwards by the virial mass as is appropriate for total mass accretion rates ($\dot{M} \propto M_{vir}^{1.25}$, Goerdt et al. 2015), we estimate rates 15 to 300× higher for 10

to 100× higher halo masses. A rough estimate suggests that the shock subtends $\sim 1\%$ of the spherical surface area at 250 kpc, and when we use the mass flow rate (Sect. 3), this implies an accretion rate per unit solid angle $\sim 2 \times 10^4 \, M_\odot \, yr^{-1} \, sr^{-1}$ – a value consistent with simulations.

Many properties of the Lyα emission we observed in the circumgalactic medium of MRC 0316-257 are broadly consistent with the results of simulations of gas accretion streams. However, we view aspects of this agreement as fortuitous. Simulations generally lack the spatial and temporal resolution necessary to capture thermal and dynamical instabilities, resolve high Mach shock fronts, fragmentation of the post-shock gas, and turbulence, which naturally occur in astrophysical gas flows (Kritsuk & Norman 2002; Cornuault et al. 2016). It is not clear if simulations show conspicuously large shock fronts and strong post-shock cooling at approximately the halo boundary, as we have suggested. Such fronts, if real, are important for establishing many properties of the gas on its inward journey deeper into the potential well (fragmenting the gas and inducing turbulence). Until simulations reach the necessary resolutions and input physics to resolve shock fronts and fragmentation, it is fair to say that our theoretical understanding of these flows is limited. Observational constraints, such as those provided here, are crucial for obtaining a deeper understanding of how galaxies obtain their gas through gas accretion flows.

References

Allen, M., Groves, B., Dopita, M., Sutherland, R., & Kewley, L. 2008, ApJS, 178, 20
Bacon, R., Accardo, M., Adjali, L., et al. 2010, in Ground-based and Airborne Instrumentation for Astronomy III, Proc. SPIE, 7735, 773508
Birnboim, Y., & Dekel, A. 2003, MNRAS, 345, 349
Cantalupo, S. 2017, in Gas Accretion onto Galaxies, Astrophys. Space Sci. Lib., 430, 195
Cantalupo, S., Porciani, C., Lilly, S. J., & Miniati, F. 2005, ApJ, 628, 61
Chambers, K. C., Miley, G. K., & van Breugel, W. J. M. 1990, ApJ, 363, 21
Christensen, L., Jahnke, K., Wisotzki, L., & Sánchez, S. F. 2006, A&A, 459, 717
Cornuault, N., Lehnert, M. D., Boulanger, F., & Guillard, P. 2016, A&A, submitted [arXiv:1609.04405]
De Breuck, C., Seymour, N., Stern, D., et al. 2010, ApJ, 725, 36
Drouart, G., De Breuck, C., Vernet, J., et al. 2012, A&A, 548, A45
Gheller, C., Vazza, F., Brüggen, M., et al. 2016, MNRAS, 462, 448
Goerdt, T., & Ceverino, D. 2015, MNRAS, 450, 3359
Goerdt, T., Dekel, A., Sternberg, A., et al. 2010, MNRAS, 407, 613
Goerdt, T., Ceverino, D., Dekel, A., & Teyssier, R. 2015, MNRAS, 454, 637
Gullberg, B., De Breuck, C., Lehnert, M. D., et al. 2016, A&A, 586, A124
Haardt, F., & Madau, P. 1996, ApJ, 461, 20
Heckman, T., Lehnert, M., Miley, G., & van Breugel, W. 1991a, ApJ, 381, 373
Heckman, T., Miley, G., Lehnert, M., & van Breugel, W. 1991b, ApJ, 370, 78
Jeng, M. 2006, Am. J. Phys., 74, 578
Kritsuk, A. G., & Norman, M. L. 2002, ApJ, 569, L127
Kuiper, E., Venemans, B. P., Hatch, N. A., Miley, G. K., & Röttgering, H. J. A. 2012, MNRAS, 425, 801
Maller, A. H., & Bullock, J. S. 2004, MNRAS, 355, 694
Martin, D. C., Chang, D., Matuszewski, M., et al. 2014, ApJ, 786, 107
Nesvadba, N., Lehnert, M., De Breuck, C., Gilbert, A., & van Breugel, W. 2008, A&A, 491, 407
Overzier, R. A., Nesvadba, N., Dijkstra, M., et al. 2013, ApJ, 771, 89
Reuland, M., van Breugel, W., Röttgering, H., et al. 2003, ApJ, 592, 755
Rosdahl, J., & Blaizot, J. 2012, MNRAS, 423, 344
Steidel, C. C., Adelberger, K. L., Shapley, A. E., et al. 2000, ApJ, 532, 170
Swinbank, A. M., Vernet, J. D. R., Smail, I., et al. 2015, MNRAS, 449, 1298
Villar-Martín, M., Vernet, J., di Serego Alighieri, S., et al. 2003, MNRAS, 346, 273
Weilbacher, P. M., Streicher, O., Urrutia, T., et al. 2012, in Software and Cyberinfrastructure for Astronomy II, Proc. SPIE, 8451, 84510B